


Nontrivial dynamics of a two-site system: Transient crystalsM. Kurzyna  and T. Kwapiński**Institute of Physics, M. Curie Skłodowska University, 20-031 Lublin, Poland*

(Received 14 August 2020; accepted 19 November 2020; published 14 December 2020)

We analyze theoretically quench dynamics of a two-site system abruptly driven from its equilibrium state focusing on the time dependent spectral density function. In the presence of electron reservoirs this function reveals in time a nontrivial regular pattern of peaks corresponding to the stationary quantum chain structure. Such dynamical system with periodic structure of the spectral density stands for a new transient crystal material. We investigate here the role of the Coulomb repulsion between the sites, nontrivial substrates and different system geometries on the transient crystal pattern which can be measured in the tunneling conductance experiments. We also propose the transient crystal system between unbiased leads as an effective monoparametric pump.

DOI: [10.1103/PhysRevB.102.245414](https://doi.org/10.1103/PhysRevB.102.245414)**I. INTRODUCTION**

Time response of a quantum system on external perturbations, transient effects, and quench dynamics have attracted considerable attention recently as they can provide much useful information about the system as well as due to potential applications of such structures in spintronics, quantum computing, or metrology. Many interesting effects were found for such systems driven by external forces like the turnstile effect, photon-assisted tunneling, spin and charge quantum pumps [1–5]. Time dependent processes may even lead to the appearance of novel solid state phases like the Floquet topological insulators [6,7] or time crystals [8–10]. In the most general sense time crystals are materials which somehow pulse or have structure behavior in time and their formation is quite analogous to the formation of space crystals [10]. However, in the presence of external periodic perturbation time crystals do not follow the period of the driving force but spontaneously switch to their own time periodicity which was confirmed experimentally [11,12].

Transient effects in atomic systems or quantum dots (QDs) have been intensively studied over recent years focusing on the charge oscillations and current dynamics (see Ref. [13] and references therein). For atomic molecules subjected to sudden perturbations (like the quenches or turnstiles) electronic and vibronic response time lies in the picosecond range like for a single semiconductor quantum dot [14,15] or for a double QD system [16]. On the other hand single-molecule devices work in the microwave regime. This motivates us to extend the molecular device investigations on the transient phenomena as the operation speed of such systems can significantly increase. A number of theoretical works studied the transient effects in different QD geometries as well as for a QD between superconducting leads [13,17,18]. The coherent oscillations and current beats for different types of time-dependent pulses can also provide an insight into the

electronic structure of such systems, e.g., from detailed studies of the transient currents one can obtain the spin relaxation time [15] or the parameters defining the system [17].

Thus far theoretical studies on transient/quench effects have been mostly focused on the current (or charge) oscillations while the quench dynamics of the spectral density function related to the quantum system has been often overlooked. The spectral density function corresponds to the local density of states (DOS) at a given site due to its coupling with the continuum electron spectra in the electrode and expresses the possible states for electrons at this site. This function determines many electronic and optical properties of the system and can be experimentally investigated by the scanning tunneling microscope (STM) from the differential conductance characteristics. In this work we concentrate on the dynamical properties of the system composed of two coupled sites on a nontrivial surface focusing on the time dependent spectral density function and its evolution due to quantum quenches or linear perturbations. We expect that such a double-site system just after the quench exchanges information between the sites and can exhibit in time a peaked regular structure of the spectral density function. In this context it is desirable to answer the question *whether a two-atom nonequilibrium system could stand for a kind of time crystal?* Next: *How fast is the structure of the spectral density built in time and then how fast does it vanish after the quench? What is a role of the electron reservoir? Is the spectral density structure periodic or does it change irregularly with time?* We would like also to determine characteristic timescales needed for the spectral density peaks to develop or to disappear. In our studies we precisely address these questions and consider different system geometries and include the Coulomb repulsion between the sites. Moreover, real 2D substrate electrodes characterized by DOS with the van Hove singularities are considered which make the problem nontrivial especially for time dependent Hamiltonian. Note that for flat DOS a wide band limit (WBL) approximation is often used which drastically simplifies mathematical derivations and leads to analytical formulas for stationary as well as for driven

*tomasz.kwapinski@umcs.pl

systems [19–21]. However, for real DOS (beyond the wide band) time dependent calculations need more sophisticated methods [21–24] and, e.g., within the Heisenberg equation of motion it is hardly possible to obtain the time-dependent local DOS. Moreover, nonequilibrium quantum systems (e.g. after the quench) between unbiased leads could be considered as monoparametric pumps. Such systems are of great interest as they involve a reduction of the system size due to a smaller number of contacts which lead to decreasing of dissipation processes in comparison with ordinary two-parameter pumps [2,4,25–34]. Additionally, monoparametric pumps eliminate dipolelike forces which appear in the presence of two or more external time-dependent fields (with a phase shift between them) [35]. Here, we propose the transient crystal system between unbiased electrodes as an effective monoparametric pump. To analyze the pumping currents, electron occupancies, and the spectral density dynamics we use a tight-binding Hamiltonian and the evolution operator technique which was successfully applied for arbitrary time dependence of external perturbations [20,21,24,36]. This method allows us to find some analytical time-dependent formulas for the evolution operator matrix elements within the Laplace transform technique.

The paper is organized as follows. In Sec. II, we describe the theoretical model and the calculation method. In Sec. III, the main results of the paper are discussed for the transient crystal. In Sec. IV the role of the real DOS structure of the electrode is analyzed; in Sec. V different system configurations are discussed. Section VI is devoted to the monoparametric pumping and the Coulomb repulsion between sites is studied in Sec. VII. The last section gives a short summary.

II. MODEL AND THEORETICAL DESCRIPTION

The model under consideration consists of two coupled electron sites (double QD, two-state system, atomic dimer) on the substrate or between external electrodes. We are going to analyze time dynamics of the spectral density related to both sites, the occupancies, and the pumping currents flowing through the system. The total time dependent Hamiltonian can be written in the second quantization notation as follows:

$$H = H_{\text{lead}} + H_0(t) + V(t), \quad (1)$$

where electrons in the leads are described by the term $H_{\text{lead}} = \sum_{\alpha} \sum_{k\alpha} \varepsilon_{k\alpha} c_{k\alpha}^{\dagger} c_{k\alpha}$, similarly the Hamiltonian for electrons at the central system takes the form: $H_0(t) = \sum_i \varepsilon_i c_i^{\dagger} c_i + U^C c_1^{\dagger} c_1 c_2^{\dagger} c_2$, and the coupling term: $V(t) = V_{12} c_1^{\dagger} c_2 + \sum_{i,k\alpha} V_{i,k\alpha}(t) c_{k\alpha}^{\dagger} c_i + \text{H.c.}$ Here $\alpha = L, R$ concerns the left or the right lead, $i = 1, 2$ describes the central sites (atoms, QDs), and $c_{k\alpha} (c_{k\alpha}^{\dagger})$, $c_i (c_i^{\dagger})$ are the electron annihilation (creation) operators at the appropriate site. The electron transition between atoms is established by V_{12} coupling and between leads and the central system by $V_{i,k\alpha}$ matrix elements. In the above Hamiltonian $\varepsilon_{k\alpha}$ stands for the electron energy spectrum of the α th lead, and ε_i represents the atomic energy levels. For simplicity each site is characterized by a single electron level with the interdot Coulomb interaction between the sites. We investigate the system dynamics due to different

time-dependent perturbations like quantum quenches or adiabatically changed coupling parameters.

The time evolution of the dimer spectral density function is described in terms of the evolution operator $U(t, t_0)$ given in the interaction representation by the following equation (we assume $\hbar = 1$):

$$\begin{aligned} i \frac{dU(t, t_0)}{dt} &= \tilde{V}(t, t_0) U(t, t_0) \\ &= U_0(t, t_0) V(t) U_0^{\dagger}(t, t_0) U(t, t_0), \end{aligned} \quad (2)$$

where $U_0(t, t_0) = T \exp(i \int_{t_0}^t dt' (H_{\text{lead}}(t') + H_0(t')))$ and T denotes the time ordering. It is assumed that for $t < t_0$ electron states in the system are decoupled and the couplings are switched on at $t = t_0$ leading to the transient effects. The electron occupation number can be obtained from the knowledge of the appropriate evolution operator matrix elements $\langle i | U | k\alpha \rangle = U_{i,k\alpha}(t, t_0)$:

$$n_i(t) = \sum_{k,\alpha} n_{k\alpha}(t_0) |U_{i,k\alpha}(t, t_0)|^2. \quad (3)$$

The spectral density function at each site (also called the local DOS) for the zero temperature can be obtained from the relation:

$$\rho_i(E, t) = \sum_{\alpha} D_{\alpha}(E) |U_{i,\alpha}(E, t, t_0)|^2, \quad (4)$$

where $D_{\alpha}(E)$ is the lead's density of states and we use the notation $U_{i,k\alpha}(t, t_0) = U_{i,\alpha}(E, t, t_0)$. In our calculations the Coulomb interdot term is considered in the form of the electrostatically interaction which in the mean field approach takes the form: $U^C c_1^{\dagger} c_1 n_2(t) + U^C c_2^{\dagger} c_2 n_1(t)$, where $n_i(t)$ is the time dependent expectation value of the appropriate site occupation. In this case the matrix elements $U_{i,k\alpha}(t, t_0)$ for $t_0 = 0$ can be obtained using Eq. (2) from the following integrodifferential Volterra equations of the second kind:

$$\begin{aligned} \frac{dU_{1,kL}(t)}{dt} &= -iV_{12} e^{iU^C(N_2(t) - N_1(t))} U_{2,kL}(t) \\ &\quad - iV_{1,kL} e^{i(\varepsilon_0 - \varepsilon_{kL})t} e^{iU^C N_2(t)} - V_{1,kL}^2 \\ &\quad \times \int_0^t dt' D_L(t-t') e^{i\varepsilon_0(t-t')} e^{iU^C \int_0^{t'} n_2(\tau) d\tau} U_{1,kL}(t'), \end{aligned} \quad (5)$$

$$\begin{aligned} \frac{dU_{2,kL}(t)}{dt} &= -iV_{12} e^{iU^C(N_1(t) - N_2(t))} U_{1,kL}(t) - V_{2,kR}^2 \\ &\quad \times \int_0^t dt' D_R(t-t') e^{i\varepsilon_0(t-t')} e^{iU^C \int_0^{t'} n_1(\tau) d\tau} U_{2,kL}(t'), \end{aligned} \quad (6)$$

where we assume the same onsite electron energies $\varepsilon_1 = \varepsilon_2 = \varepsilon_0$, and $N_i(t) = \int_0^t n_i(t') dt'$. Here $D_{\alpha}(t-t') = \int d\varepsilon D_{\alpha}(\varepsilon) \exp(-i\varepsilon(t-t'))$ is the Fourier transform of the electron density of states in the α th electrode. The similar differential relations can be written for $U_{i,kR}(t)$ elements. To find the solution for the evolution operator as a function of time it is necessary to know the charge occupations $n_i(t)$ which are obtained from the knowledge of $U_{i,k\alpha}(t)$ elements. Thus, the problem is not trivial and in general analytical solutions of

these equations do not exist. Moreover, the Fourier transforms of the lead DOS, $D(t - t')$, appearing in the right hand side of Eq. (5) and Eq. (6), have no analytical form for arbitrary $D(E)$ (besides some symmetrical DOS functions, like, e.g., the rectangular or Lorentzian DOS). Thus in general we solve the integrodifferential equations [Eqs. (5) and (6)] numerically for a given leads DOS. However, for some specific system parameters, using the Laplace transformation technique, we can obtain some interesting analytical relations and discuss them in the text.

The current flowing from the surface electrode can be obtained from the time derivative of the total number of electrons in this lead:

$$j_L(t) = -e \frac{d}{dt} \sum_{kL} n_{kL}(t), \quad (7)$$

where the electrode occupation, $n_{kL}(t)$, is expressed similarly to Eq. (3) by $U_{k\alpha, k'\alpha'}(t, t_0)$ matrix elements which satisfy the set of integrodifferential equations in the form of Eq. (5) and Eq. (6).

III. 1D TRANSIENT CRYSTAL

In this section we consider a two-site system coupled via the first site with only one (left, L) electrode such that the second site is decoupled from the lead (vertical geometry). For such a case, using Eq. (5) and Eq. (6) and for no Coulomb repulsion, $U^C = 0$, one can write the following set of differential equations for $U_{i,kL}(t)$ elements:

$$\begin{aligned} \frac{dU_{1,kL}(t)}{dt} &= -iV_{12}U_{2,kL}(t) - iV_{1,kL}e^{i(\varepsilon_0 - \varepsilon_{kL})t} - \frac{\Gamma}{2}U_{1,kL}(t) \\ \frac{dU_{2,kL}(t)}{dt} &= -iV_{12}U_{1,kL}(t), \end{aligned} \quad (8)$$

where $\Gamma = \Gamma_L = 2\pi \sum_{kL} |V_{1,kL}|^2 \delta(E - \varepsilon_{kL})$, i.e., the structureless DOS of the surface electrode is assumed (wide band approximation). The above set of differential equations can be resolved analytically using the Laplace transformation method, $\mathcal{L}\{U_{i,kL}(t)\} = F_i(s)$, which leads to the following solutions for the transformed functions:

$$\begin{aligned} F_1(s) &= \frac{-isV_{1,kL}}{(s - s_0)(s - s_1)(s - s_2)} \\ F_2(s) &= \frac{-VV_{1,kL}}{(s - s_0)(s - s_1)(s - s_2)}, \end{aligned} \quad (9)$$

where $s_0 = i(\varepsilon_0 - \varepsilon_{kL})$ and $s_{1/2} = -\frac{\Gamma}{4} \pm \sqrt{\frac{\Gamma^2}{4} - 4V^2}$. In this case the inverse Laplace transformation for $F_i(s)$ can be calculated analytically and after some algebra one obtains time-dependent evolution operator matrix elements:

$$\begin{aligned} U_{1,kL}(t) &= \frac{-iV_{1,kL}s_0}{(s_0 - s_1)(s_0 - s_2)} e^{s_0 t} + \frac{-iV_{1,kL}s_1}{(s_1 - s_0)(s_1 - s_2)} e^{s_1 t} \\ &+ \frac{-iV_{1,kL}s_2}{(s_2 - s_0)(s_2 - s_1)} e^{s_2 t}, \end{aligned} \quad (10)$$

and similar for $U_{2,kL}(t)$ elements, where one should change $-iV_{1,kL}s_i$ into $-V_{12}V_{1,kL}$ in all nominators in the above equation. It is worth noting that the first part of the above relation oscillates in time while the second and third terms vanish

nonmonotonically due to the exponent functions with s_1 and s_2 (which real parts are negative). Analytical solutions for $U_{i,kL}(t)$ evolution operator matrix elements within the WBL allow us to obtain the current form Eq. (7):

$$\begin{aligned} j_L(t) &= -2Im \left\{ \sum_{kL} n_{kL}(0) V_{kL} e^{i(\varepsilon_{kL} - \varepsilon_0)t} U_{1,kL}(t) \right\} \\ &- \Gamma n_1(t), \end{aligned} \quad (11)$$

where $n_{kL}(0)$ stands for the initial occupation of electron states in the electrode which is related to the Fermi distribution function, and we assume $e = 1$. The relations for $U_{i,kL}(t)$, Eq. (10), have a more transparent form for $\varepsilon_{kL} = \varepsilon_0 = 0$, which can be written as follows (we define $x = \frac{\Gamma}{4V_{12}}$):

$$\begin{aligned} U_{1,kL}(t) &= \frac{-iV_{1,kL}}{V\sqrt{x^2 - 1}} e^{-\frac{\Gamma}{4}t} \sinh(V_{12}\sqrt{x^2 - 1}t), \\ U_{2,kL}(t) &= \frac{-V_{1,kL}}{V_{12}} + \frac{-V_{1,kL}}{V_{12}} e^{-\frac{\Gamma}{4}t} \\ &\times \left\{ \cosh(V_{12}\sqrt{x^2 - 1}t) \right. \\ &\left. + \frac{x}{\sqrt{x^2 - 1}} \sinh(V_{12}\sqrt{x^2 - 1}t) \right\}. \end{aligned} \quad (12)$$

These analytical relations for $U_{i,kL}(t)$ allow us to analyze time dynamics of the spectral density functions at both sites. In our calculations all energies are expressed in the units of $\Gamma_L = \Gamma \equiv 1$, time in \hbar/Γ units (which for $\Gamma = 1$ meV equals 0.6 ps), and the energy reference point is the left electrode Fermi energy, $E_F = 0$, moreover a shortened notation of the site-site coupling $V_{12} = V$ is used.

In the beginning we analyze dynamical formation in time of the spectral density function for $\Gamma_L = 1$, $\Gamma_R = 0$ (vertical geometry). In Fig. 1 we show the local DOS dynamics related to the second site, $\rho_2(E, t)$, for different values of the site-site coupling parameter, $V = 0.4, 2, 4$, and 8, from the upper to bottom panel, respectively. The quench takes place at $t = 0$ (for $t < 0$ we have $V = 0$, $\Gamma_\alpha = 0$) and for $t \rightarrow \infty$ the spectral density corresponds to the stationary case, i.e., it is characterized by two peaks localized for $E = \pm V$. These peaks for relatively small V parameter overlap each other which is visible in the upper panel (for $V = 0.4$). It results directly from Eq. (12) where for $t \rightarrow \infty$ the evolution operator matrix element for the Fermi energy $E = 0$ does not vanish, $U_{2,kL} = \frac{-V_{1,kL}}{V}$, and thus $\rho_2(E = 0, t \rightarrow \infty) \sim \frac{V_{1,kL}^2}{V^2}$. It means that the spectral density function at the Fermi level vanishes for larger V but for smaller V (for $x > 1$, i.e., for $\Gamma > 4V$) it monotonically increases after the quench (without oscillations). For larger values of V ($x < 1$) the spectral function $\rho_2(E, t)$ reveals an interesting structure as a function of time (see three bottom panels in Fig. 1). In the beginning one wide peak of $\rho_2(E, t)$ appears and for large t only two side peaks at $E = \pm V$ are observed which stand for the steady solution of the double-site system. However, as a main feature of this quench we observe interference patterns of the spectral density function between the main stationary DOS peaks. These patterns come from the evolution in time of the spectral density at both sites in the presence of the electron reservoir.

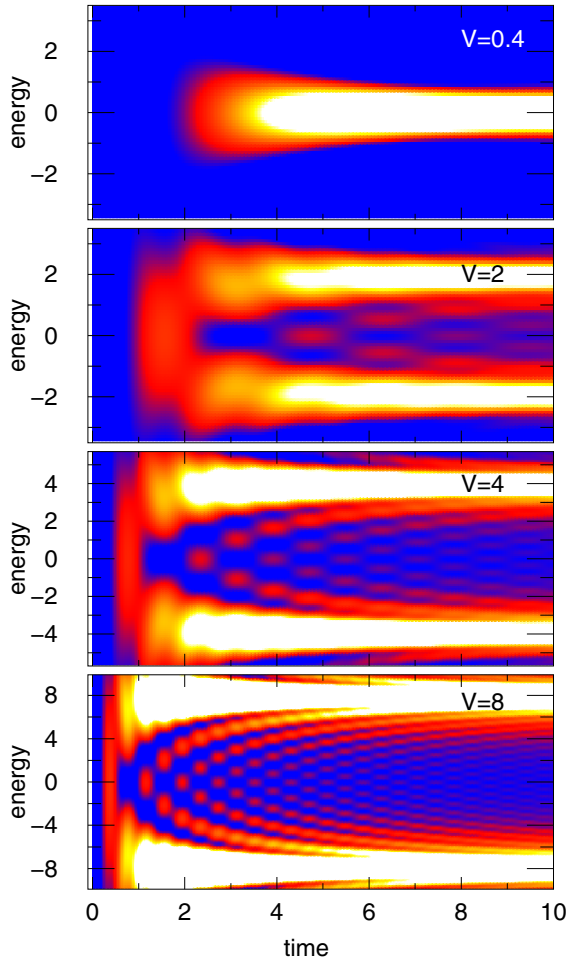


FIG. 1. Spectral density function $\rho_2(E, t)$ of the two-site system after the quench at $t = 0$ (for $t < 0$: $\Gamma_{L/R} = 0$ and $V = 0$). For $t > 0$ the site-site coupling is $V = 0.4, 2, 4$, and 8 (from upper to bottom panels, respectively) and $\Gamma_L = 1$. The other parameters are $\Gamma_R = 0$, $V_{1,kL} = 4$, $V_{2,kL} = V_{1,kR} = V_{2,kR} = 0$, $\varepsilon_0 = 0$, $U^C = 0$. The units of all energies and time are $\Gamma_L = \Gamma$ and \hbar/Γ , respectively.

Due to the coupling with the substrate just after the quench a single DOS peak at the first site appears. This information, after some time, reaches the second site, and its spectrum, $\rho_2(E, t)$, broadens leading to a single-peak DOS structure at this site—in the second panel ($V = 2$) it appears for $t = 1.5$. Next, the spectral density function at the second site is rebuilt due to the presence of the first site and two-peaked DOS structure is observed for a moment, for $t = 3.1$. However, the system is not in its equilibrium state (it is just after the quench) and still evolves in time—the spectral density peaks become narrower and this information bounces between both sites leading (for a short period of time) to appearance of a three-state spectral density function with maximal value of DOS at the Fermi level (for $t = 4.7$), then four-state DOS (for $t = 6.3$) and so on. This process repeats again and again and one observes M -site dynamical structure of DOS in the double-site system (see also the third and fourth bottom panels). This structure, however, vanishes with time as the system tends to the equilibrium state with two-peaked spectral density function. The substrate acts here as a dissipative electrode

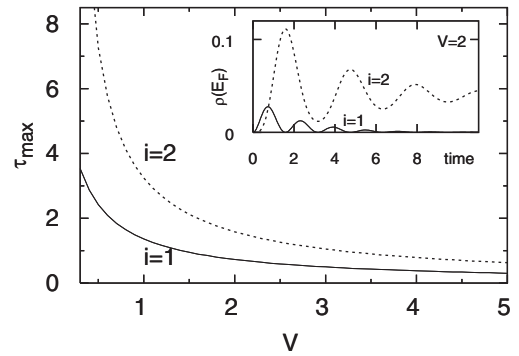


FIG. 2. Time of the first maximum in $\rho_i(E, t)$ as a function of the coupling parameter V for $i = 1$ (solid curve) and $i = 2$ (broken curve). The inset shows time evolution of the spectral density function at the Fermi level for $V = 2$ and $i = 1$ and 2 , respectively. The other parameters are the same as in Fig. 1; τ_{\max} is expressed in the time units, \hbar/Γ .

thus nonequilibrium oscillations vanish in time. The internal patterns of the dynamical local DOS correspond to the structure of DOS (or the conductance) of 1D stationary atomic chain, cf. Fig. 1 from Ref. [37], i.e., for a given time it is characterized by the structure of the M -site chain. Thus the two-site system after the quench has structure behavior in time, which stands for a kind of 1D transient crystal material. Of course this structure is quasiperiodic which means that it pulses/changes in time in a very regular way. Note that for the dimer decoupled from the leads such structure of the transient crystal does not appear and only regular and nonvanishing in time Rabi oscillations are observed.

It is worth mentioning that just after the quench the spectral density does not change immediately but there is some delay time until the information about continues electron states in the electrode reaches the second site. This time interval depends on the coupling between both sites and it decreases with increasing V , cf. the upper and bottom panels in Fig. 1 for $t = 2.5$ and 0.25 , respectively. We analyze this process in Fig. 2 where we define the delay time of the spectral density function, τ_{\max} , as a time at which $\rho_{1/2}(E, t)$ reaches its first maximum. In the insight in Fig. 2 we show the time evolution of the density functions at both sites corresponding to the Fermi level ($E = E_F = 0$) for $V = 2$. Note that the spectral density oscillates in time with the period equals $T = \frac{\pi}{V\sqrt{1-x^2}}$ and with decreasing amplitude. For these $\rho_{1/2}(E, t)$ curves the first maximum appears for $\tau_{\max} = 0.7$ (the first site) and $\tau_{\max} = 1.5$ (the second site). One expects that τ_{\max} for the first site, which is directly coupled with the electrode, should not depend on the site-site coupling, V , as the information from the substrate flows only through the coupling parameter $V_{1,kL}$ (or Γ_L). Surprisingly, this conclusion is invalid and the appearance of the first maximum at this site depends on the coupling with the second site (decoupled from the electrode). It can be confirmed by analytical calculations of the spectral density functions $\rho_1(E_F, t)$ and $\rho_2(E_F, t)$. From Eq. (12) we calculate the positions of the first maxima which for $i = 1$ can be expressed as: $\tau_{\max} = \frac{\ln(x + \sqrt{x^2 - 1})}{V\sqrt{x^2 - 1}}$ for $x > 1$ and $\tau_{\max} = \frac{\arctan(\sqrt{1-x^2}/x)}{V\sqrt{1-x^2}}$ for $x < 1$, and similar for $i = 2$. These functions

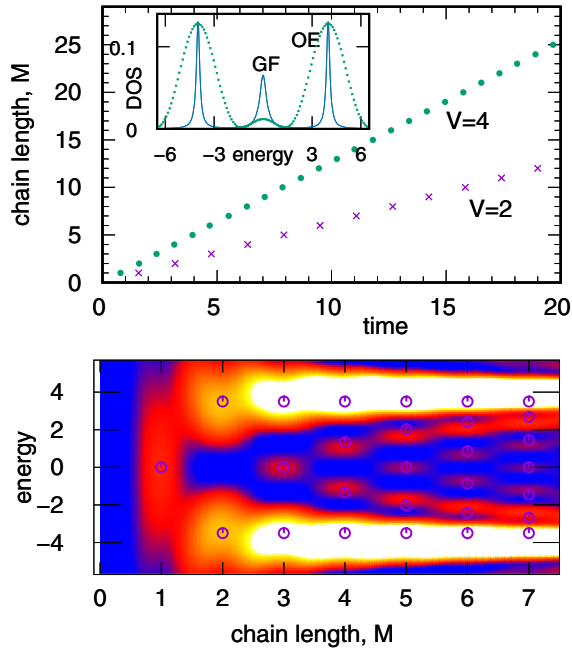


FIG. 3. (Upper panel) Effective chain length, M , as a function of time for the system described in Fig. 1 for $V = 4$ (dots) and $V = 2$ (crosses). The inset figure shows the spectral density function (normalized DOS) obtained for $M = 3$ linear sites within the Green function method with the effective coupling, $V_M = 2.83$, $\varepsilon_i = 0$ (solid curve) and for the dimer taken at time $t = 2.3$ after the quench for $V = 4$ (dotted curve). The bottom panel shows time dependent spectral density function for $V = 4$ with indicated effective chain lengths, M . The circles correspond to maxima of equilibrium DOS obtained for M -site linear chain for $V_M = V/2.3 \cos(\frac{\pi}{M+1})$. The other parameters are the same as in Fig. 1.

in both cases depend on the site-site coupling parameter, V , which is visible in Fig. 2 and in general the time delay decreases monotonically with V . It is interesting that from the knowledge of τ_{\max} one can estimate the coupling parameter between the sites. Moreover, the difference in time delay between both sites $\Delta\tau$ (between the broken and solid curves in Fig. 2) is responsible for the time travel of the information between these sites. This quantity can be derived analytically and has relatively transparent form:

$$\Delta\tau = \frac{4}{\sqrt{4V^2 - \Gamma^2}} \left(\frac{\pi}{2} + \arcsin \frac{\Gamma}{4V} \right). \quad (13)$$

One can see that for large value of V , the difference $\Delta\tau$ is very small and tends to zero (two-site system stands for a strongly coupled molecule, $V > V_{1,kL}$) but for smaller V it increases rapidly. It is worth noting that this function depends nonlinearly on the site-site coupling.

The spectral density function of the double-site system reveals a regular pattern of peaks (transient crystal) which correspond to a chain of the effective length M . It is desirable to analyze how this effective chain length M changes in time after the quench in this system. To tackle this problem we study the positions of peaks of the spectral density function in time and adjust them to the effective chain length. The results are depicted in Fig. 3 (upper panel) for $V = 2$ (crosses) and $V = 4$ (dots). It is well visible that this dependence is

linear for both cases. The linearity of $M(t)$ is a consequence of constant information rate which bounces between the sites. We have found that the structure of the effective chain length M appears for $t = \frac{2\pi M}{\sqrt{(2V)^2 - \Gamma^2}}$ and, e.g., the local DOS corresponding to $M = 5$ chain length exists in the two-atom system for $t = 8.1$ ($V = 2$) after the quench. Moreover, for weaker couplings V the effective chain length increases much slower than for larger V (which is also visible in Fig. 1 where peaks' density changes with V). It allows us to observe M -sites structure of the double-site system even for larger times.

In the inset in Fig. 3 we compare the structure of stationary DOS obtained for $M = 3$ sites chain with the dimer spectral density function captures at time $t = 2.3$ for $V = 4$. Here the Green function (GF) method was used for the model composed of a linear chain on the substrate with the same electron energies, ε_0 , and uniform effective site-site couplings, V_M . The stationary spectral density is obtained from the knowledge of the imaginary part of the site Green function, $DOS_i(E) = -\frac{1}{\pi} \text{Im} G_{ii}^r(E)$, and G_{ii}^r is found from the equation of motion for the retarded Green functions, cf., e.g., Ref. [37]. We have found that the positions of DOS peaks in the energy scale agree for both models. The differences result from the system dynamics after the quench, i.e., the intensities of the inside peaks as well as their widths for the two-site system change dynamically in time leading (for large time) to the equilibrium two-peaked structure of DOS. The general correspondence between the spectral density function of the double-site system and the M -site linear chain is shown in the bottom panel in Fig. 3. Here, on the transient crystal pattern we overplot the positions of the local DOS peaks assigned to the steady chain of the length M (circles in the bottom panel). As one can see the agreement between the dynamical structure of the two-atom system and static 1D chain DOS is quite satisfying.

IV. BEYOND THE WIDE BAND LIMIT

The transient crystal pattern appears for the two-state system after the quench in the presence of continuum electron states. In real physical systems the electron reservoir can be characterized by nontrivial band structure with peaks (van Hove singularities), gaps, or surface states. For such systems the wide band limit approximation fails and one should describe lead electrons in a more adequate way which is a nontrivial task especially for time dependent studies [21–24]. Therefore in this section we consider a more realistic model of the lead DOS as it can strongly modify the spectral density of the double-site system. We will check whether the spectral density pattern for the dimer survives in the presence of real structure of the surface DOS. In our calculations we take into consideration three different cases of the lead DOS structure shown in Fig. 4. There are: a rectangular DOS (curve A), 2D-tight binding with a single van Hove peak in the middle of the band (curve B), and DOS with two van Hove peaks with a local minimum in the middle of the band (curve C). The last two curves correspond to the 2D tight-binding rectangular and honeycomb (hexagonal) lattice which have analytical forms expressed in terms of the elliptic integrals of the first kind [38,39]. Note that in our calculations beyond the WBL one needs the time transform of DOS [as in Eq. (5) and Eq. (6)]

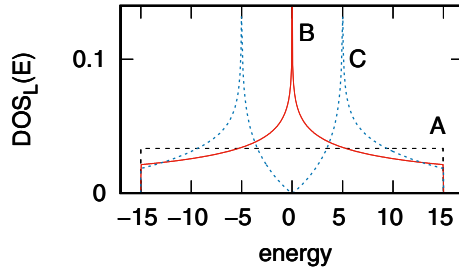


FIG. 4. Electrode density of states considered in the calculations: rectangular DOS (curve A), 2D square lattice DOS with the van Hove singularity (curve B), and 2D honeycomb (hexagonal) lattice DOS with two van Hove singularities (curve C) [38,39]. The energy unit is Γ , all curves are normalized to 1, and each DOS width is $w = 30\Gamma$.

and, e.g., for the rectangular DOS, $D(E) = \frac{\Theta(w/2 - |E|)}{w}$, (w is the DOS bandwidth and Θ is the Heaviside step function), the time Fourier transform has a simple analytical solution, $D(t) = \frac{\sin(tw/2)}{tw/2}$.

The spectral density function for the double-site system coupled vertically with the lead (surface electrode) described by different DOS structures is shown in Fig. 5 (A, B, and C, from the upper to bottom panels). As one can see the rectangular DOS of the electrode slightly modifies in time the spectral density pattern of the system in comparison with the results obtained within the wide band approximation, cf. Fig. 1, the third panel for $V = 4$. It results from the fact that the rectangular DOS can be well substituted by the wide band structure especially for energies lying in the middle of the band. For the surface DOS with the van Hove singularity in the middle of the band, panel B, one observes clear amplification of peaks intensities in the structure of the spectral density function. This effect results from larger values of DOS of the surface band near the Fermi level in comparison with the rectangular DOS, cf. Fig. 4. Thus the transient crystal can be observed for such DOS structure even for larger times. The situation changes for two van Hove singularities in DOS, panel C (hexagonal lattice). In this case the dimer spectral density near the Fermi level is strongly reduced due to low surface DOS at the Fermi level and the spectral density pattern is hardly visible. It is worth noting that the spectral density peaks appear at the same energies and at the same time for all considered surface DOS. Thus the surface structure does not influence the transient crystal pattern in general but can change its intensity.

V. OTHER CONFIGURATIONS

In this section we study the role of different geometries of the system on 1D transient crystal patterns. First in Fig. 6 we consider a linear change of the site-site coupling from zero to $V = 4$ within 5 time units (between $t = 10$ and $t = 15$). Thus we assume that there is a single site at the electrode and at a given time, $t = 10$, the second site is coupled with it. As one can see the evident peaked pattern of the spectral density appears with decreasing intensities. The first spectral density peak which appears just after $t = 10$ is broadened and exists longer in time than for the sudden quench. Moreover, one observes a linear change of the main DOS peaks in time

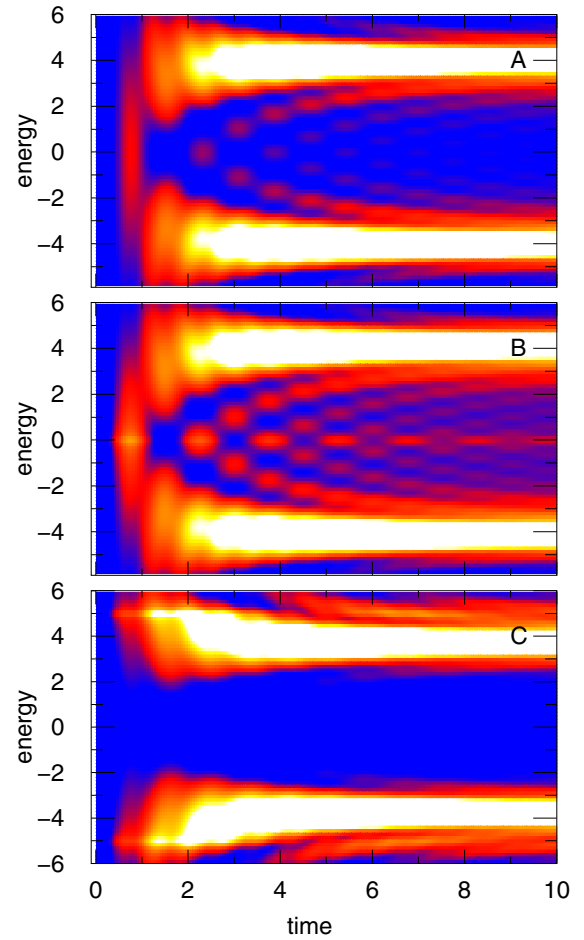


FIG. 5. Spectral density function $\rho_2(E, t)$ of the two-site system coupled vertically with the lead characterized by different DOS shown in Fig. 4, curves A, B, and C (upper, middle, and bottom panel, respectively). The other parameters are the same as in Fig. 1, $V = 4$.

(tilted white ridges) up to the time when the site-site coupling is constant. It is the reason that the structure of 1D transient crystal with DOS peaks is slightly squeezed in the energy scale and shifted in time.

Thus far we have investigated two-site systems in the vertical geometry at the surface. In real situations they can

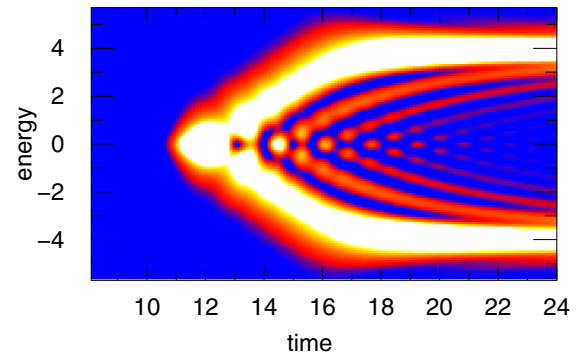


FIG. 6. Spectral density function $\rho_2(E, t)$ for linear change of V from $V = 0$ (at $t = 10$) up to $V = 4$ (for $t \geq 15$). The other parameters are the same as in Fig. 1.

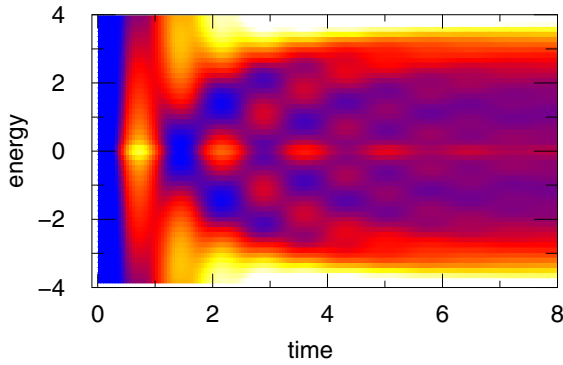


FIG. 7. Spectral density function of the two-site system in the horizontal geometry $\rho_2(E, t) = \rho_1(E, t)$ after the quench with the substrate characterized by 2D tight-binding DOS with a van Hove peak in the middle of the band. The other parameters are the same as in Fig. 1, $V = 4$, $V_{1,kL} = V_{2,kR} = V_k = 2.82$.

be also coupled horizontally or can be situated between two electrodes (as for a DQD system). In this case the evolution operator matrix elements $U_{i,kL}(t)$ needed to obtain the spectral density satisfy similar equations to Eq. (8) [for this horizontal geometry in the second equation one should add the term: $-\frac{\Gamma}{2}U_{2,kL}(t)$], and for the wide band approximation and symmetrical couplings $\Gamma_L = \Gamma_R = \Gamma$ ($V_{1,kL} = V_{2,kR} = V_k$) we can obtain the Laplace transformations for the evolution operator elements: $F_1(s) = -iV_k(s + \frac{\Gamma}{2})/N$, and $F_2(s) = -VV_k/N$, where $N = [s - i(\varepsilon_0 - \varepsilon_k)](s + \frac{\Gamma}{2} - iV)(s + \frac{\Gamma}{2} + iV)$. After some algebra the inverse Laplace transformations for them can be obtained as follows (for $\varepsilon_k = E_F = 0$):

$$\begin{aligned}
 U_{1,kL}(t) &= \frac{-iV_k}{\left(\frac{\Gamma}{2}\right)^2 + V^2} \\
 &\quad \times \left(\frac{\Gamma}{2} - e^{-\frac{\Gamma}{2}t} \frac{\Gamma}{2} \cos(Vt) + Ve^{-\frac{\Gamma}{2}t} \sin(Vt) \right) \\
 U_{1,kR}(t) &= \frac{V_k}{\left(\frac{\Gamma}{2}\right)^2 + V^2} \\
 &\quad \times \left(-V - e^{-\frac{\Gamma}{2}t} \frac{\Gamma}{2} \sin(Vt) + Ve^{-\frac{\Gamma}{2}t} \cos(Vt) \right)
 \end{aligned} \tag{14}$$

and the spectral density function at the Fermi level (which is the same for both sites) can be written in the following form:

$$\rho_{1/2}(t) = \frac{1}{2\pi} \frac{1}{V^2 + \left(\frac{\Gamma}{2}\right)^2} (1 + e^{-\Gamma t} - 2e^{-\frac{\Gamma}{2}t} \cos(Vt)). \tag{15}$$

It is interesting that in this case the oscillation period of $\rho_i(E, t)$ is exactly the same as for the isolated dimer system (Rabi oscillations), i.e., $T = 2\pi/V$. Apparently, for the system decoupled from the substrate these oscillations do not vanish in time but here due to nonzero Γ parameter they exponentially decrease. Note that the oscillations of the spectral density in the horizontal geometry are also observed for other nonconstant surface DOS (for which analytical formulas do not exist). In Fig. 7 we show the results for the two-site

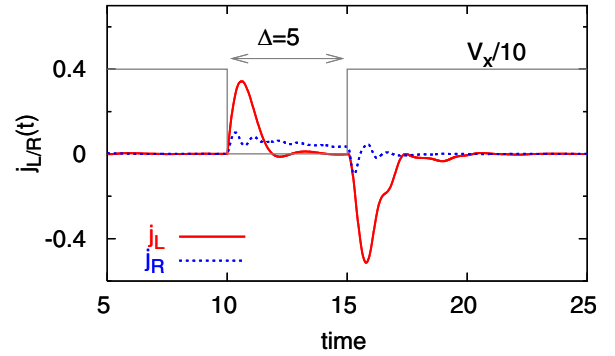


FIG. 8. Time dependent currents flowing from the left (red solid curve) and from the right (blue broken curve) electrodes for $\varepsilon_0 = -2$. The coupling $V = 4$ was switched off at $t = 10$ for a period of $\Delta = 5$ time units (black dotted line). The left (right) electrode is characterized by 2D-TB DOS with one (two) van Hove singularity (see Fig. 4), both DOS are symmetrical and their widths are $w = 50$ energy units, the current unit is $e\Gamma/\hbar$.

horizontal system coupled with the lead (surface electrode) described by the 2D tight-binding DOS with the van Hove singularity at the Fermi level. As one can see the transient crystal pattern is well visible in this case with a larger intensity of peaks for $E \simeq 0$ related to the van Hove singularity at the Fermi level. As before, the oscillation period of $\rho_i(E, t)$ corresponds to the Rabi oscillations.

VI. MONO-PARAMETRIC PUMPING

We have shown that a two-site system coupled with the electrode reveals regular oscillations for a short period of time after the quench. During this time the system is out of equilibrium thus it can be proposed as an effective monoparametric electron pump. In doing so we consider two electron sites between unbiased leads and change nonadiabatically in time only the site-site coupling parameter, V . In Fig. 8 we analyze the left and right currents flowing through such a system for suddenly vanishing in time coupling strength V at $t = 10$ and switched on again at $t = 15$, as is indicated by the broken black curve. The system is space symmetrical but here we consider two different density of states of the left and right leads, i.e., with one (left lead) or two (right lead) van Hove singularities, Fig. 4. It leads to asymmetry which is crucial for the pumping effect (in the case of the same structure of the left and right DOS electrons are not pumped through the system). Before the perturbation, $t < 10$, the spectral density of the two-site system is characterized by two peaks localized below and above the Fermi energy (in our case at $E = \varepsilon_0 \pm V = -6, +2$) thus both sites are almost half occupied. At $t = 10$ the sites are decoupled and the local DOS is transformed to a single peak DOS with the maximum at $E = \varepsilon_0 = -2$ which lies below the Fermi energy. In this case the occupancies of both sites increase and the electrons flow from the leads to the sites (the currents are positive). It is evident that for the electrode with larger DOS around the Fermi energy this process occurs much faster (red curve) in comparison with the electrode with low DOS (E_F), blue curve. At $t = 15$ the sites are coupled together again and their spectral density evolves

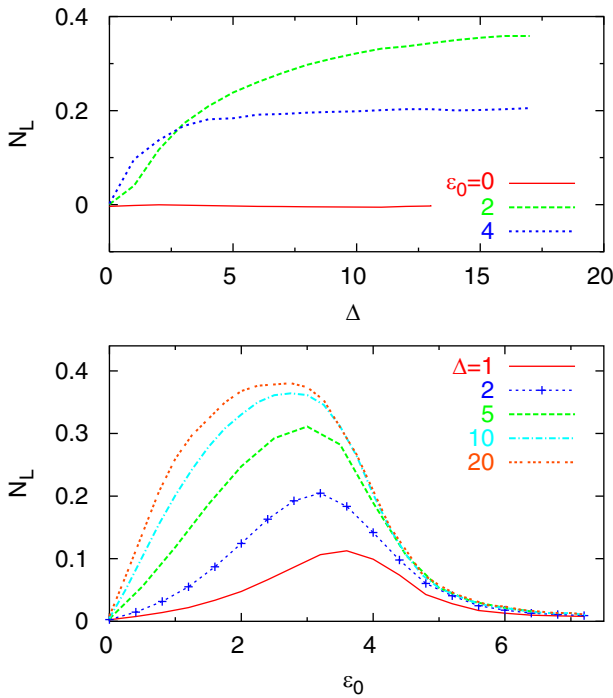


FIG. 9. Pumped charge through the two-site system between the unbiased leads during the changing of V parameter (shown in Fig. 8) as a function of Δ for $\varepsilon_0 = 0, 2, 4$ (upper panel) and as a function of ε_0 for $\Delta = 0, 2, 5, 10, 20$ (bottom panel). The unit of Δ is \hbar/Γ .

in time to the same structures as before the quench (with two peaks of DOS lying below and above the Fermi energy). This is the reason that some excess charge, related to the state below the Fermi energy, has to leave the sites and the current is negative. After about 5 time units from the quench ($t > 20$) the system reaches its steady state and the currents vanish. During this process the transient crystal pattern appears at both sites as was discussed in Fig. 7 but the left and right sites are charged/discharged with different rates, e.g., the right site is charged very slowly due to low DOS of the right lead at the Fermi energy. Thus after the quench (for $t > 15$) the excess charge flows to the right electrode (very slowly) but also to the left electrode through the first site. Nonuniform charge migration after the quench leads to electron pumping in the double-site system using only one time dependent parameter (monoparametric pumping) and it is desirable to analyze this phenomenon in more details.

The net charge flowing from the left/right electrode can be calculated by integration of the time-dependent currents, i.e., $N_{L/R} = \int j_{L/R}(t) dt$. We assume only one cycle of $V(t)$ variations shown in the upper panel in Fig. 8, and obtain the net charge, N_L , flowing from/to the left electrode (extension to periodic cycles is straightforward). Both sites are decoupled during the period of Δ and the system is in the same equilibrium state before and after the perturbation. First we are interested how Δ parameter influences the pumping charge and in Fig. 9, upper panel, we show the charge flowing from the left electrode, N_L , as a function of Δ for various onsite energies, ε_0 . As one can see for $\Delta = 0$ electrons do not flow through the system (there is no quench). For nonzero Δ and symmetrical local DOS at both sites (symmetrical versus the

Fermi energy) the net charge also does not flow (red line). However, in the presence of asymmetry in the local DOS ($\varepsilon_0 = 2, 4$) green and blue curves) the charge is pumped and increases for small Δ . For larger Δ it tends to some constant value which means that for this perturbation maximal charge is pumped through the system. Note also that for negative ε_0 the charge is pumped from the right to the left electrode and for positive ε_0 the current direction is opposite. Thus the gate voltage can effectively control the electron current direction in the system.

In order to reveal further the role of the onsite energies on the pumping current we analyze in the bottom panel of Fig. 9 the net charge as a function of ε_0 for different Δ parameter indicated in the legend. As before for $\varepsilon_0 = 0$ (symmetrical case) the charge is not pumped through the system independently of Δ . Also for large ε_0 electrons are not transferred between electrodes because there are no local DOS peaks at the Fermi level in both sites. Maximal pumped charge is observed for average values of ε_0 when there is asymmetry in the spectral density function and simultaneously there is nonzero DOS at the Fermi level. The pumped charge depends on the Δ parameter—for small Δ maximal N_L appears for $\varepsilon_0 \simeq V$ which corresponds to the local DOS peak at the Fermi energy but for larger Δ the system reaches its steady state after each change of V and maximal value of N_L is observed for $\varepsilon_0 = V/2$.

VII. TRANSIENT CRYSTAL PATTERN IN THE PRESENCE OF THE COULOMB REPULSION

Electron correlations in low dimensional systems can play an important role leading to, e.g., the Kondo effect, Coulomb blockade, spin-charge separation, and others. However, in many real atomic structures the correlation effects are marginal and can be omitted (like for Pb atoms on vicinal surfaces [40]) or can be described effectively as an electrostatic coupling between charged electron sites. In this section we consider the Coulomb electrostatic coupling between the sites and check whether the Coulomb repulsion influences or destroys the transient crystal pattern. In general, even for the wide-band approximation analytical solutions of Eqs. (5) and (6) do not exist. However, in the limit of small U^C , e.g., for the two-site system coupled only with one electrode, instead of the integrodifferential Volterra equations of the second kind we have the following ones:

$$\begin{aligned} \frac{dU_{1,kL}(t)}{dt} &= -iV e^{iU^C(n_2(t)-n_1(t))t} U_{2,kL}(t) \\ &\quad - iV_{1,kL} e^{i(\varepsilon_0 + U^C n_2(t) - \varepsilon_{kL})t} - \frac{\Gamma}{2} U_{1,kL}(t) \\ \frac{dU_{2,kL}(t)}{dt} &= -iV e^{iU^C(n_1(t)-n_2(t))t} U_{1,kL}(t). \end{aligned} \quad (16)$$

Unfortunately, due to the time dependent occupations, $n_i(t)$, the Laplace transform technique cannot be applied to find analytical solutions. Further approximations, like the assumption that $n_i(t)$ does not depend on time [only in the RHS of Eq. (16)] lead to unphysical effects. Thus in the paper we consider finite values of U^C and show the results obtained numerically for small U^C and wide band approximation

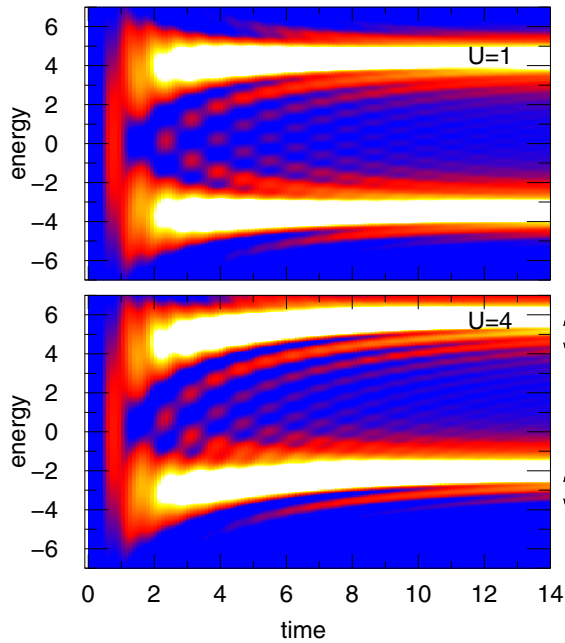


FIG. 10. Time dependent spectral density function of the two-site system after the quench at $t = 0$ for small Coulomb repulsion between sites $U^C = 1$ (upper panel) and for the stronger one, $U^C = 4$, (bottom panel). The arrows indicate the energy shifting of the stationary peaks of the local DOS due to the Coulomb repulsion. The other parameters are the same as in Fig. 1, $V = 4$.

according to Eq. (16) and for larger U^C and beyond the WBL (rectangular lead DOS) using Eq. (5) and Eq. (6).

In order to reveal the role of the Coulomb repulsion on the transient crystal pattern we analyze in Fig. 10 the spectral density function for weak electron-electron repulsion, $U^C = 1$ (upper panel), and for $U^C = 4$ (bottom panel). As one can see the structure of $\rho_2(E, t)$ for small U slightly differs from that from Fig. 1 obtained for $U^C = 0$ and for $V = 4$. However, for larger U^C we observe that the spectral density is shifted and the main DOS peaks for $t \rightarrow \infty$ appear for $E = \pm V + U^C n(t)$: The occupation number in our case tends to 0.5 thus $U^C n(t) \rightarrow 2$ which was indicated in Fig. 10 by the arrows. It leads to modifications of the spectral density pattern but the transient crystal structure of the local DOS peaks is still visible. Note that similar behavior of the conductance spectra (shifting towards higher energies) was observed for N -site linear chain in the presence of the Coulomb interactions

obtained within the slave boson and mean-field techniques [41]. Here this effect holds in time for only the two-site system which additionally confirms its relation with the DOS structure behavior of 1D chains.

VIII. CONCLUSIONS

In this work we have studied the dynamical properties of a system composed of two coupled sites focusing on the time dependent spectral density function and its evolution due to quantum quenches and linear perturbations. Using the evolution operator technique and tight-binding Hamiltonian we have found that the spectral density function reveals a very regular structure of peaks in the time domain. This peaked pattern oscillates in time, and it corresponds to a quantum chain density of states with increasing chain length. Thus it stands for a new material which is characterized by the pulsed structure changing regularly in time. This transient crystal exists for nonequilibrium systems (e.g., after the quench) and vanishes as the system tends to its steady state so it cannot be classified strictly as a time crystal. We have also shown that the predicted pattern of the transient crystal could be observed for two-site systems on different electrodes with the van Hove singularities as well as for different system geometries. Additionally, we have found that in the presence of the Coulomb repulsion between sites the spectral density function is shifted towards higher energies but the transient crystal pattern is still visible in the system.

Moreover, using the series of quantum quenches we propose an effective monoparametric pump based on the transient crystal system between unbiased leads. In the presence of two different lead DOS, by changing in time only the coupling parameter between the sites, the net electron charge can be transferred in the system. In this case the transient crystal pattern appears together with the pumping current whose direction can be determined by the gate voltage potential.

It is believed that our results will bring new perspectives to a wide range of time-dependent crystals. They can be verified experimentally using time spectroscopy techniques or in photonic crystals.

ACKNOWLEDGMENTS

This work was partially supported by National Science Centre, Poland, under Grant No. 2018/31/B/ST3/02370.

-
- [1] T. H. Oosterkamp, L. P. Kouwenhoven, A. E. A. Koolen, N. C. van der Vaart, and C. J. P. M. Harmans, *Phys. Rev. Lett.* **78**, 1536 (1997).
 - [2] L. P. Kouwenhoven, A. T. Johnson, N. C. van der Vaart, A. van der Enden, C. J. P. M. Harmans, and C. T. Foxon, *Z. Phys. B-Condensed Matter* **85**, 381 (1991).
 - [3] R. H. Blick, R. J. Haug, J. Weis, D. Pfannkuche, K. v. Klitzing, and K. Eberl, *Phys. Rev. B* **53**, 7899 (1996).
 - [4] S. K. Watson, R. M. Potok, C. M. Marcus, and V. Umansky, *Phys. Rev. Lett.* **91**, 258301 (2003).
 - [5] G. Platero and R. Aguado, *Phys. Rep.* **395**, 1 (2004).
 - [6] N. H. Lindner, G. Refael, and V. Galitski, *Nat. Phys.* **7**, 490 (2011).
 - [7] G. Usaj, P. M. Perez-Piskunow, L. E. F. Foa Torres, and C. A. Balseiro, *Phys. Rev. B* **90**, 115423 (2014).
 - [8] F. Wilczek, *Phys. Rev. Lett.* **109**, 160401 (2012).
 - [9] K. Sacha, *Phys. Rev. A* **91**, 033617 (2015).

- [10] K. Sacha and J. Zakrzewski, *Rep. Prog. Phys.* **81**, 016401 (2017).
- [11] S. Choi, J. Choi, R. Landig, G. Kucsko, H. Zhou, J. Isoya, F. Jelezko, S. Onoda, H. Sumiya, V. Khemani, C. von Keyserlingk, N. Y. Yao, E. Demler, and M. D. Lukin, *Nature (London)* **543**, 221 (2017).
- [12] J. Zhang, P. W. Hess, A. Kyprianidis, P. Becker, A. Lee, J. Smith, G. Pagano, I.-D. Potirniche, A. C. Potter, A. Vishwanath, N. Y. Yao, and C. Monroe, *Nature (London)* **543**, 217 (2017).
- [13] R. Taranko, T. Kwapiński, and T. Domański, *Phys. Rev. B* **99**, 165419 (2019).
- [14] T. Fujisawa, Y. Tokura, and Y. Hirayama, *Phys. Rev. B* **63**, 081304(R) (2001).
- [15] T. Fujisawa, D. G. Austing, Y. Tokura, Y. Hirayama, and S. Tarucha, *J. Phys.: Condens. Matter* **15**, R1395 (2003).
- [16] T. Hayashi, T. Fujisawa, H. D. Cheong, Y. H. Jeong, and Y. Hirayama, *Phys. Rev. Lett.* **91**, 226804 (2003).
- [17] E. Taranko, M. Wiertel, and R. Taranko, *J. Appl. Phys.* **111**, 023711 (2012).
- [18] T. Kwapiński and R. Taranko, *Physica E* **63**, 241 (2014).
- [19] A.-P. Jauho, N. S. Wingreen, and Y. Meir, *Phys. Rev. B* **50**, 5528 (1994).
- [20] R. Taranko, T. Kwapiński, and E. Taranko, *Phys. Rev. B* **69**, 165306 (2004).
- [21] Y.-Q. Zhou, R.-Q. Wang, L. Sheng, B. Wang, and D. Y. Xing, *Phys. Rev. B* **78**, 155327 (2008).
- [22] J. Maciejko, J. Wang, and H. Guo, *Phys. Rev. B* **74**, 085324 (2006).
- [23] Y. Zhu, J. Maciejko, T. Ji, H. Guo, and J. Wang, *Phys. Rev. B* **71**, 075317 (2005).
- [24] T. Kwapiński, R. Taranko, and E. Taranko, *Phys. Rev. B* **66**, 035315 (2002).
- [25] M. Switkes, C. M. Marcus, K. Campman, and A. C. Gossard, *Science* **283**, 1905 (1999).
- [26] B. Roche, R.-P. Riwar, B. Voisin, E. Dupont-Ferrier, R. Wacquez, M. Vinet, M. Sanquer, J. Splettstoesser, and X. Jehl, *Nat. Commun.* **4**, 1581 (2013).
- [27] L. E. F. Foa Torres, *Phys. Rev. B* **72**, 245339 (2005).
- [28] M. G. Vavilov, L. DiCarlo, and C. M. Marcus, *Phys. Rev. B* **71**, 241309(R) (2005).
- [29] L. DiCarlo, C. M. Marcus, and J. S. Harris, *Phys. Rev. Lett.* **91**, 246804 (2003).
- [30] L. E. F. Foa Torres, H. L. Calvo, C. G. Rocha, and G. Cuniberti, *Appl. Phys. Lett.* **99**, 092102 (2011).
- [31] T. Aref, V. F. Maisi, M. V. Gustafsson, P. Delsing, and J. P. Pekola, *Europhys. Lett.* **96**, 37008 (2011).
- [32] P. San-Jose, E. Prada, S. Kohler, and H. Schomerus, *Phys. Rev. B* **84**, 155408 (2011).
- [33] Y. Zhou and M. W. Wu, *Phys. Rev. B* **86**, 085406 (2012).
- [34] T. Kwapiński and R. Taranko, *Eur. Phys. J. B* **88**, 140 (2015).
- [35] S. Kohler, J. Lehmann, and P. Hänggi, *Phys. Rep.* **406**, 379 (2005).
- [36] T. Grimley, V. Jyothi Bhasu, and K. Sebastian, *Surf. Sci.* **121**, 305 (1983).
- [37] T. Kwapiński, *J. Phys.: Condens. Matter* **17**, 5849 (2005).
- [38] T. C. Choy, *Phys. Rev. Lett.* **55**, 2915 (1985).
- [39] T. Horiguchi, *J. Math. Phys.* **13**, 1411 (1972).
- [40] M. Jałochowski, T. Kwapiński, P. Łukasik, P. Nita, and M. Kopciuszynski, *J. Phys.: Condens. Matter* **28**, 284003 (2016).
- [41] M. Krawiec and T. Kwapiński, *Surf. Sci.* **600**, 1697 (2006).